Applied Chemical Engineering (2024) Volume 7 Issue 1
doi: 10.24294/ace.v7i1.2236

ORIGINAL RESEARCH ARTICLE

Probing Ti–doped (Al–Ga) surface as Nanosensor for adsorbing the S- & N-containing heterocyclic compounds

Fatemeh Mollaamin[1,*], Majid Monajjemi[2]

[1] *Department of Biomedical Engineering, Faculty of Engineering and Architecture, Kastamonu University, Kastamonu 37150, Turkey*

[2] *Department of Chemical engineering, Central Tehran Branch, Islamic Azad University, Tehran 1496969191, Iran*

*** Corresponding author:** Fatemeh Mollaamin, smollaamin@gmail.com

ABSTRACT

Aluminum–Gallium doped with titanium by using ONIOM method through structural, electrical, and thermodynamic properties was studied in detail. Crystal structure of Ti–(Al–Ga) surface was coated by S- & N-heterocyclic carbenes of benzotriazole (BTA), 2-mercaptobenzothiazole (2MBT), 8-hydroxyquinoline (8HQ) and 3-amino-1,2,4-triazole-5-thiol (ATR). The "NMR" spectroscopy of the adsorption of BTA, 2MBT, 8HQ, and ATR on the Ti–doped Al–Ga nanoalloy surface represents that this surface can be employed as the magnetic S- & N-heterocyclic carbene sensors. In fact, "Ti" site in "Ti–(Al–Ga)" nanoalloy surface has bigger interaction energy amount from "Van der Waals' forces" with BTA, 2MBT, 8HQ, and ATR that might cause them large stable towards coating data on the nanosurface. It has been estimated that the criterion for choosing the surface linkage of "S" and "N" atom in BTA, 2MBT, 8HQ, and ATR in adsorption sites can be impacted by the existence of close atoms of aluminum and gallium in the "Ti–(Al–Ga)" surface. The fluctuation of "NQR" has estimated the inhibiting role of BTA, 2MBT, 8HQ, and ATR for Ti–doped Al–Ga alloy nanosheet due to "S" and "N" atoms in the benzene cycle of heterocyclic carbenes being near the monolayer surface of ternary "Ti–(Al–Ga)" nanoalloy. Moreover, "IR" spectroscopy has exhibited that Ti–doped Al–Ga alloy nanosheet with the fluctuation in the frequency of intra–atomic interaction leads us to the most considerable influence in the vicinage elements generated due to inter–atomic interaction. Comparison to ΔG^{o}_{ads} amounts versus dipole moment has illustrated a proper accord among measured parameters based on the rightness of the chosen isotherm for the adsorption steps of the formation of BTA @Ti–(Al–Ga), 2MBT @Ti–(Al–Ga), 8HQ @Ti–(Al–Ga), and ATR @Ti–(Al–Ga) complexes. Thus, the interval between sulfur, nitrogen and oxygen atoms in BTA, 2MBT, 8HQ, and ATR during interaction with transition metal of "Ti" in "Ti–(Al–Ga)" nanoalloy, (N→Ti, O→Ti, S→Ti), has been estimated with relation coefficient of $R^2 = 0.9509$. Thus, the present has exhibit the influence of "Ti" doped on the "Al–Ga" surface for adsorption of S- & N-heterocyclic carbenes of BTA, 2MBT, 8HQ, and ATR by using theoretical methods. Furthermore, the "partial electron density" or "PDOS" has estimated a certain charge assembly between Ti–(Al–Ga) and S– & N–heterocycles of BTA, 2MBT, 8HQ, and ATR which can remark that the complex dominant of metallic features and an exact degree of covalent traits can describe the augmenting of the sensitivity of "Ti–(Al–Ga)" surface as a potent sensor for adsorption of BTA, 2MBT, 8HQ, and ATR heterocycles.

Keywords: (S- & N-heterocycles) @(Ti–Al–Ga) complexes; BTA, 2MBT, 8HQ, ATR; DFT; Langmuir adsorption; CAM-B3LYP/EPR-III, LANL2DZ,6-31+G(d,p)

1. Introduction

The Material selection is one of the popular approaches used to prevent corrosive reactions. Apart from special needs joint to the real application and the corrosion environment, there are also usual factors to be denoted in material selection[1]. The alloys of metal elements are employed in the branches of car designing, national defense society, airplane industry, electronics and daily significant building with high quality[2]. As a matter of fact, Al material is generated by Hall-Héroult approach with defects of high energy consumption,

ARTICLE INFO

Received: 12 June 2023
Accepted: 11 September 2023
Available online: 4 January 2024

rigid corrosion of instruments, environmental pollution and other issues[3,4].

In fact, heterocyclic organic compounds consisting of multiple bonds and heteroatoms like oxygen, nitrogen and sulfur are remarkable corrosion inhibitors owing to the absorbance on the metal surface through their heteroatoms. The adsorption of heterocyclic organic compounds on the metal surface closes active zones and decreases the speed of corrosion. Nevertheless, the efficiency of the inhibitor is related to the physico-chemical attributes such as inhibitor structure, being special functional groups, aromaticity, different types of corrosive solutions and charge electron density[5–8].

It is obvious that heterocyclic carbenes containing “S” and “N” atoms are impressible corrosion compounds for diverse series of metals in varied acidic solutions[9–16]. Since various specifications of heterocycles carbenes are remarked, it is crucial that the electrons of a series of heterocycles are considered. Thus, functionalized heterocycles as corrosion inhibiting agents have been selected and identified based on their physico-chemical specifications, and an attention has been assigned to the quantitative assessment of the internal and steric impact of these structures upon their inhibiting output[17–22]. It has been seen that heterocycles containing “S” and “N” atoms are appropriate corrosion inhibiting agents for most of metal crystals in diverse acidic conditions; For example benzotriazole at the “Cu” and “Fe” electrode, isoquinoline and imidazole families at the “Fe” electrode are impressive inhibiting agents for corrosion of these metal crystals[23–39]. The microscopic interaction and reaction mechanism between molecules might be deeply revealed from the quantum chemical specifications which provide an advantageous track to detect adsorption tendency between molecules and interfaces at the atomic and molecular stages[40–42]. Nowadays, it has been shown that pyridine and alkylpyridines had been employed as corrosion inhibiting agents of the “Al” crystal. There are many investigations that have been devoted to the usage of potent heterocycles and heteroatomic molecules consisting of organic materials that enhance the anticorrosion qualifications of metal surfaces and alloys. The presence of heteroatoms containing “O, S, N, P” atoms, “aromatic rings” and “multiple bonds” with “π–electrons” in these inhibiting agents support largely the foundation of inactive blocks on metal crystal and alloys[43–48]. Moreover, it has been analyzed that alkylpyridines have been widely used through their strong polarity which enhances in ionic liquids and solution media.

There is a reasonable connection between the thickness of the passive layer and the effectiveness of inhibiting the corrosion action[49,50]. From the XRD patterns and impedance spectroscopy, it was found that gallium replaces AlT, AlO, and Ti sites in the

NASICON $LiTi_2(PO_4)_3$ (LTP) phase. The formation of TiO_2, $AlPO_4$, and $GaPO_4$ phases are explained on basis of XRD, and conductivity enhancement of Li^+ due to presence of Ga^{3+} and Al^{3+} near the (M1 and M2) cation vacancy sites is explained. The Ga^{3+} is likely to replace Al and Ti–both cations. From the impedance scaling, it was determined that the presence of different phases near grain boundary also influenced the conductivity with increase in content of gallium[51].

In the previous works, the adsorption analysis of pyridine, and nitrogen heterocyclic derivatives onto pristine two-layer aluminum surface[52], pure monolayer aluminum metal surface based on Freundlich Adsorption[53] have been investigated. Furthermore, the data of Langmuir adsorption model of organic inhibitors containing pyridine and alkylpyridines[54]; BTA, 8HQ, and 2MBT[55] by using monolayer binary alloys of the "Al–Mg", "Al–Ga", "Al–Si" surfaces have been reported. Besides, the role of pyridine and its family compounds as corrosion inhibiting agents for monolayer ternary "Al" nanoalloys including "Al–Mg–Si", "Al–Mg–Ge", "Al–Mg–Sn" surfaces have been studied[56].

Now, the present work intends to extend the previous works[52–56] toward the investigation of Ti–doped "Al–Ga" surface for adsorption of S- & N-heterocyclic carbenes of benzotriazole (BTA), 2-mercaptobenzothiazole (2MBT), 8-hydroxyquinoline (8HQ) and 3-amino-1,2,4-triazole-5-thiol (ATR) by using through "CAM-B3LYP/EPR-III, LANL2DZ,6-31+G(d,p)" theoretical methods.

2. Theoretical Insights, applied material and method

2.1. Ti–doped Al–Ga alloy & inhibitory

Certain of the popular kinds of corrosion for "Al" which are autonomous of the corrosive condition contain "pitting", "stress-corrosion cracking", "exfoliation", "intergranular", and "galvanic"[57]. The non-heat manageable alloys have the larger corrosion persistence against common corrosion compared to the heat manageable alloys. "Al–alloys" might be sensitive to intergranular corrosion process if "second-phase" micro components are generated at grain boundary orientations. A corrosion ability of the alloy is separate from that of the matrix will also make intergranular corrosion process. The existence of perceptible values of soluble alloying elements like "Cu, Mg, Si, and Zn" will cause these alloys sensitive to "stress-corrosion" cracking process[58,59]. Certain elements like Cu and Mg added to Al alloys ameliorate the mechanical attributes and conduct the alloy to reply the heat dealing. The existence of magnesium also increases resistance and reduces the rate of strength loss at high temperature in the alloys.

Aluminum–Gallium (Al–Ga) which is a degenerate alloy is obtained from liquid gallium diffusing the crystal structure of Ga metal. This alloy is so much fragile that is broken under a little pressure. Al–Ga alloy is also chemically more fragile, because it prevents Al from forming a protective oxide layer. This element and its alloys are usually employed experimental fluids for modeling both liquid and solid dynamics in planetary cores. Al–Ga is able to react with H_2O molecules to produce Al oxide, Ga metal and hydrogen gas. Al reacts in air to generate an inactive layer of aluminum oxide and it doesn't react with water. Aluminum–Gallium alloy can form Al nanoparticles for the hydrogen creating reaction[60].

In this article, the adsorption of BTA, 2MBT, 8HQ, ATR as corrosion inhibitors on the Ti–(Al–Ga) surface was coated by S- & N-heterocyclic carbenes of benzotriazole (BTA), 2-mercaptobenzothiazole (2MBT), 3-amino-1,2,4-triazole-5-thiol (ATR), and 8-hydroxyquinoline (8HQ) was assigned by the most suitable Langmuir isotherm, which exhibits the chemisorptive nature of the bond between the inhibitor molecules and the Ti–(Al–Ga) alloy surface (**Figure 1**).

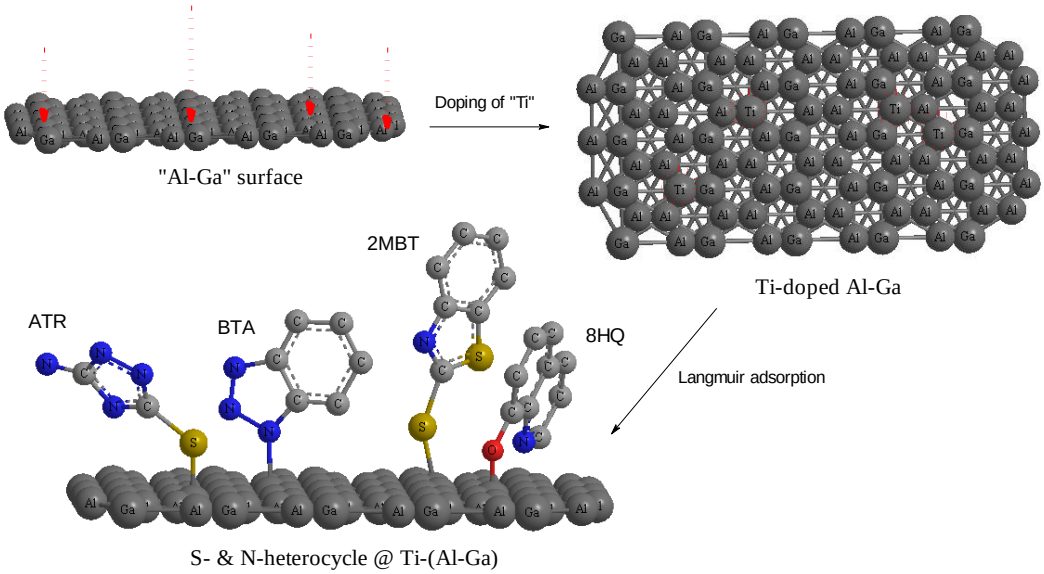

Figure 1. Introduction of physico-chemical adsorbing properties of S- & N-heterocyclic carbenes of BTA, 2MBT, 8HQ, ATR onto Ti–(Al–Ga) alloy.

2.2. Multilayer & multilevel of theoretical "ONIOM" approach

From computational level of "ONIOM" methodology, any combination of three levels in the decreasing the order of accuracy might be confirmed in "ONIOM3". The specially admissible levels are "high QM1", "medium QM2", and "low QM3 or MM", where "high level QM1" frequently is the "ab–initio" or "DFT" methodology, "medium level QM2" is a "low–level ab initio", "DFT", or "semi–empirical (SE) QM" methodology, and low level includes an "SE QM" methodology or the "MM" methodology[61].

Based on this research, "ONIOM" methodology, "QM" has been performed due to the "DFT" methodology of "CAM–B3LYP" with "6-31+G(d,p)" basis set for "H", "C", "S" and "O" atoms, EPR-III for "N" atom and "LANL2DZ" for the transition metals of "Ti" atom in the adsorption sites. "QM2" has been fulfilled on certain "Al" and "Ga" atoms in the adsorption sites due to semi-empirical force fields. And, a "QM3" has been discussed on the other "Al" and "Ga" atoms with "MM2" methodology (**Figure 1**)[61].

Therefore, the mixing of three levels of "QM", "QM2" and "QM3" in decreasing the order of validity has been allocated possessing "high", "medium", and "low" surfaces of theoretical level[62]:

$$E_{\text{ONIOM}} = E_{\text{high(QM1)}} + E_{\text{medium(QM2)}} + E_{\text{low(QM3)}} \quad (1)$$

"ONIOM" as a "three–layered" methodology of authorizes us to unravel a bigger system more explicitly than the "one-layered" model which may behave a medium size system stringently like a huge system with usual exactitude (**Figure 1**)[63]. So, the mentioned "three–layered" sample has been used to activate barriers for the BTA, 2MBT, 8HQ, ATR onto mono-layer Ti–(Al–Ga) alloy surface towards generating the "Langmuir adsorption" complexes consisting of BTA @Ti–(Al–Ga), 2MBT @Ti–(Al–Ga), 8HQ @Ti–(Al–Ga), and ATR @Ti–(Al–Ga) (**Figure 1**).

2.3. Density Functional Theory (DFT) Method

Our computations have been carried out due to the conceptual "DFT" using the projector enhanced wave "PAW"[64] methodology. The Perdew–Burke–Ernzerhof "PBE" functional under the generalized gradient approximation "GGA"[65] was applied as the "exchange-correlation" functional. The nonempirical "PBE" functional is recognized to relegate precise crystal specifications[66]. Commonly, where "GGA" functionals lose out, local density functionals stop too. Considering the thermal conductivity compared to local density functionals, "PBE" does not over attach structures, and therefore the interatomic force constants are not too flexible. All in all, the lattice thermal conductivity is entirely the same whether using local density or "GGA"

functionals[67–73].

"DFT" or "Density functional theory" calculations have been accomplished by using "Gaussian 16 revision C.01" program package[74]. The input Z–matrix for the S- & N-heterocyclic carbenes of BTA, 2MBT, 8HQ, ATR as corrosion inhibiting agents adsorbed onto the "Ti–(Al–Ga)" alloy surface (**Figure 1**) has been provided with "GaussView 6.1"[75] due to the rigid system and coordination format of which a blank line has been cited and using "LANL2DZ,EPR–III, 6-31 + G(d,p)" basis sets to distinguish "chemical shielding", "frequencies", "thermodynamic properties", "electrostatic and electronic potential", "natural atomic charges, "projected density of state" and other quantum properties for this work. The rigid "PES" has been calculated at "CAM–B3LYP/EPR–III,LANL2DZ,6-31 + G(d,p)" for (BTA, 2MBT, 8HQ, ATR) adsorbed onto "Ti–(Al–Ga)" alloys surface in which the small energy difference between the formations of "BTA @ TM–(Al–Ga), 2MBT @ TM–(Al–Ga), 8HQ @ TM–(Al–Ga), and ATR @ TM–(Al–Ga) complexes can direct us to an efficient coated crystal for preventing the corrosion process. Thus, it has been discovered that the crystal binding site preferable of "N, O, S-atoms" is largely impacted by the essence of neighboring "N, O, S–atoms". The calculated "(BTA, 2MBT, 8HQ, ATR) @ Ti–(Al–Ga)" pair repartition functions have predicted that the formation of crystals addresses to shorter "N→Ti–alloy, O→Ti–alloy, and S→Ti–alloy" bond lengths when it is figured out to the analogous growth (**Figure 1**).

3. Results and discussion

The adsorption of BTA, 2MBT, 8HQ, ATR as S- & N-heterocyclic carbenes on the "Al–Ga" Nanoalloy doped with Ti in "NaCl" solution was allocated by the most appropriate "Langmuir isotherm", which remarks the "chemisorptive" nature of the bond among the (BTA, 2MBT, 8HQ, ATR) @TM–(Al–Ga) complexes, the equilibrium distribution of ions of the adsorbing compound between the solid and liquid phases, and a monolayer attribute. The adsorbed molecules are kept on the "Ti–(Al–Ga)" surface with chemisorbed inhibitors having high protection (**Figure 1**).

3.1. The Properties of Electronic specification

The electronic structures of BTA, 2MBT, 8HQ, ATR adsorbed on the Ti–doped Al–Ga surface have been investigated to simplify subsequent study for interfacial electronic properties using "CAM-B3LYP/ LANL2DZ, 6-311+G (d,p)" basis sets.

Figure 2a–d shows the projected density of state "PDOS" of the (BTA, 2MBT, 8HQ, ATR) @Ti–Al–Ga surface. The appearance of the energy states (*d*-orbital) of Ti within the gap of Al–Ga surface induces the reactivity of the system. It is clear from the figure that after doping with Ti atom, there is a significant contribution of "Ti" *d*-orbital in the unoccupied level. Based on the population analysis and "DOS", it can be concluded that "Ti" remains in the cationic state and it can accept more electrons from other atoms. Therefore, the curve of partial "DOS (PDOS)" has described that the "*p* states" of the adsorbing process of "S" & "N" atom of on the BTA, 2MBT, 8HQ, ATR adsorbed on the "Ti–(Al–Ga)" surface are overcoming due to the conduction band (**Figure 2a–d**). A distinguished metallic trait might be seen in BTA, 2MBT, 8HQ, ATR @"Ti–(Al–Ga)" crystal because of the potent interaction between the "*p* states" of C, N, O, S, Al, Ga and the "*d*" state of "Ti" near the "Fermi energy". Furthermore, the essence of covalent traits for these clusters has displayed the similar energy value and image of the "PDOS" for the "*p* orbitals" of C, N, O, S, Al, Ga and "*d* orbitals" of "Ti" (**Figure 2a–d**).

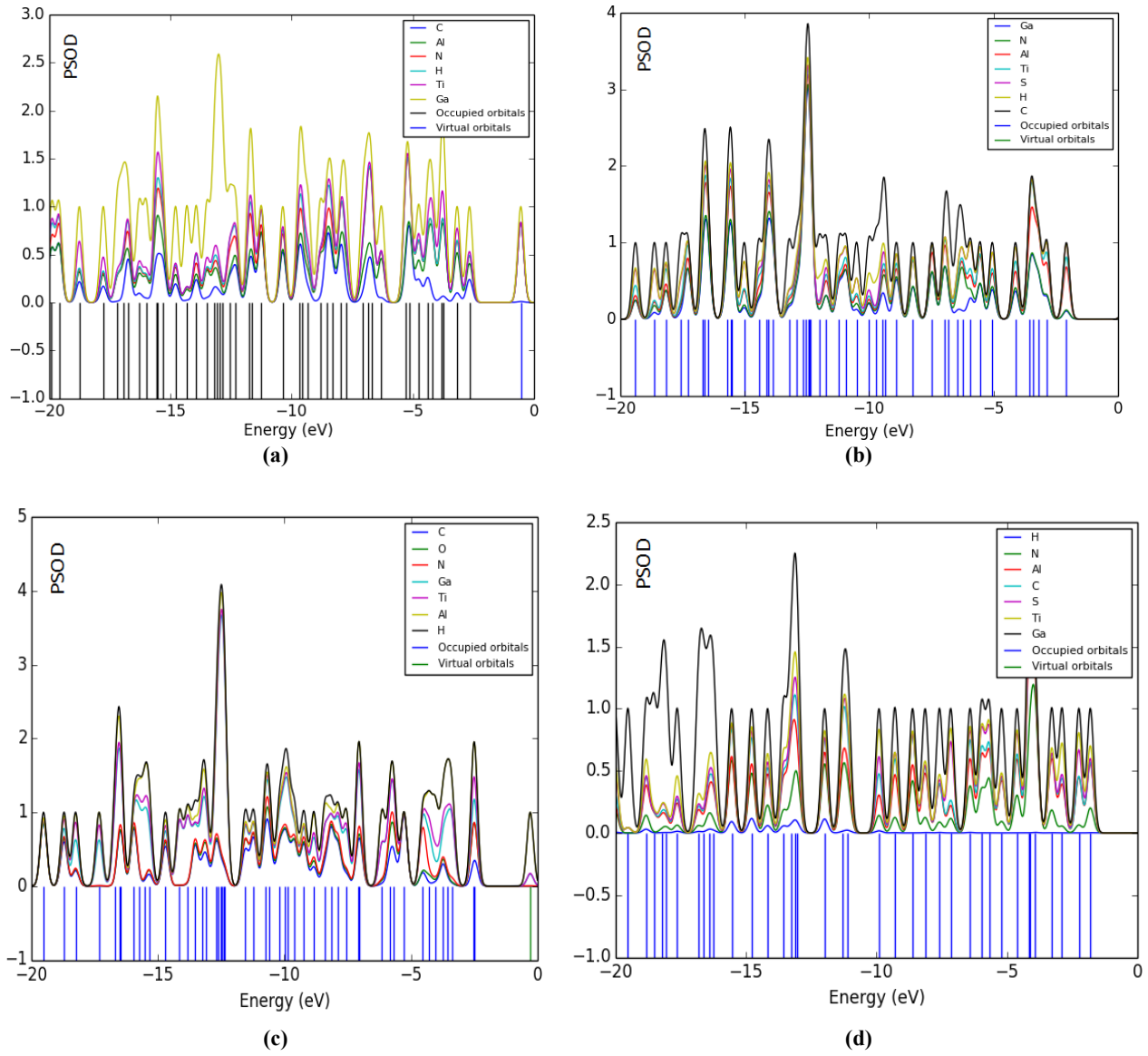

Figure 2. "PDOS" adsorption of **(a)** BTA @ Ti–(Al–Ga), **(b)** 2MBT @ Ti–(Al–Ga), **(c)** 8HQ @ Ti–(Al–Ga), and **(d)** ATR @ Ti–(Al–Ga) with Fermi level = 0.

Figure 2a–d shows that the BTA @ Ti–(Al–Ga), 2MBT @ Ti–(Al–Ga), 8HQ @ Ti–(Al–Ga), and ATR @Ti–(Al–Ga) states, respectively, have the most contribution at the middle of the conduction band between −5 to −20 eV. Contribution of gallium states in BTA @" Ti–(Al–Ga) complex are enlarged, but hydrogen, carbon, nitrogen, aluminum, and titanium states have little contributions and similar together (**Figure 2a**). Furthermore, contribution of hydrogen, carbon, nitrogen, sulfur, aluminum, and titanium in 2MBT @" Ti–(Al–Ga) complex are enlarged and similar together (**Figure 2b**). Moreover, contribution of hydrogen, carbon, oxygen, aluminum, and titanium in 8HQ @Ti–(Al–Ga) complex are enlarged and similar together, but nitrogen states have little contributions (**Figure 2c**). Beside, contribution of gallium states in ATR @Ti–(Al–Ga) complex are enlarged, but hydrogen, carbon, nitrogen, sulfur, aluminum, and titanium states have little contributions and similar together (**Figure 2d**).

The "partial electron density" or "PDOS" can also estimate a certain charge assembly between Ti–(Al–Ga) and S- & N-heterocycles of BTA, 2MBT, 8HQ, and ATR. On the other hand, the above data can illustrate that the complex dominant of metallic features and an exact degree of covalent traits can describe the augmenting of the sensitivity of "Ti–(Al–Ga)" surface as a potent sensor for adsorption of BTA, 2MBT, 8HQ, and ATR heterocycles (**Figure 2a–d**).

3.2. Magnetism and atomic charge analysis

Nuclear magnetic resonance spectrum of Ti–doped "Al–Ga" alloy surface as the potent sensor for adsorbing the S- & N-heterocycles of BTA, 2MBT, 8HQ, and ATR can unravel the role of the indicated transition metal of "Ti" in the active site of "Al–Ga" alloy surface through the formation of the covalent binding between S- & N-heterocyclic carbenes (adsorbate) and surface (adsorbent).

From the "DFT" calculations, it has been attained the "chemical shielding" (CS) tensors in the principal axes system to estimate the "isotropic chemical-shielding" (CSI) and "anisotropic chemical–shielding" (CSA)[76]:

$$\sigma_{iso} = (\sigma_{11} + \sigma_{22} + \sigma_{33})/3 \quad (2)$$

$$\sigma_{aniso} = \sigma_{33} - (\sigma_{22} + \sigma_{11})/2 \quad (3)$$

The chemical shielding extracts from "Nuclear magnetic resonance" or "NMR" can be applied for allocating the structural and geometrical specifications of materials. As a matter of fact, "Gauge Invariant Atomic Orbital" or "GIAO" methodology has been recommended as a valid methodology for "NMR" parameter computations and "ONIOM" has caught much regards for gaining "NMR" chemical shielding of "inhibitor-surface" complexes such as isotropic chemical shielding appears in Equation (4):

$$\sigma_{iso,ONIOM} = \sigma_{iso,high(QM1)} + \sigma_{iso,medium(QM2)} + \sigma_{iso,low(QM3)} \quad (4)$$

The "NMR" data of isotropic "σ_{iso}" and anisotropic shielding tensor "σ_{aniso}" for BTA @Ti–(Al–Ga), 2MBT @Ti–(Al–Ga), 8HQ @Ti–(Al–Ga), and ATR @Ti–(Al–Ga) complexes have been computed by "Gaussian 16 revision C.01" program package[74] and been shown in **Table 1**.

Table 1. NMR properties of chemical shielding tensors (σ_{iso} & σ_{aniso}/ppm) for BTA @Ti–(Al–Ga), 2MBT @Ti–(Al–Ga), 8HQ @Ti–(Al–Ga), and ATR @Ti–(Al–Ga) complexes.

BTA @Ti–(Al–Ga)			**2MBT @Ti–(Al–Ga)**			**8HQ @Ti–(Al–Ga)**			**ATR @Ti–(Al–Ga)**		
Atom	**σ_{iso}**	**σ_{aniso}**	**Atom**	**σ_{iso}**	**σ_{aniso}**	**Atom**	**σ_{iso}**	**σ_{aniso}**	**Atom**	**σ_{iso}**	**σ_{aniso}**
C1	115.7400	167.1911	C1	138.2183	120.7762	C1	115.6284	97.1211	N1	66.2666	220.1213
C2	123.1077	146.5940	C	134.0515	133.5171	C2	129.4094	131.1109	C2	108.9951	89.1839
C3	123.1391	115.5774	C3	152.8493	79.9594	C3	123.2336	121.0239	C3	93.3383	37.4125
C4	105.7168	63.6944	C4	130.4395	68.8030	C4	125.1511	159.7292	N4	145.5038	308.3332
C5	128.0957	134.6295	C5	135.8676	128.6658	C5	130.7512	118.3958	N5	56.5231	181.7100
C6	125.2577	134.5757	C6	129.2949	138.9273	C6	117.9570	147.8562	N6	273.4976	40.0943
N7	138.1353	142.9835	S7	810.8707	208.1817	N7	5.4087	485.5466	S7	862.5215	494.6408
N8	34.6360	142.6484	C8	105.6628	185.5172	C8	108.2072	128.4342	Al8	254.3320	575.3041
N9	33.1241	320.6595	N9	83.7001	298.0337	C9	125.0637	140.8585	Ga9	370.3780	650.3940
Ga10	2579.9301	407.8428	S10	676.0546	555.3818	C10	119.9337	134.8668	Al10	352.4745	533.3908
Al11	480.1440	410.9498	Ga11	2386.5752	622.1167	O11	274.9979	639.6289	Ga11	2335.8966	765.5075
Ga12	1118.3269	1161.1280	Al12	392.0125	407.3028	Ga12	2699.3615	203.5223	Al12	216.2356	728.7044
Al13	72.4557	539.3687	Ga13	1412.9832	782.5463	Al13	462.4740	321.0927	Ga13	369.9747	960.5613
Al14	98.1250	455.8092	Al14	163.1344	544.0216	Ga14	1119.0769	1129.0216	Ti14	690.0063	1038.2717
Ga15	1661.1119	525.1091	Al15	268.8910	174.8583	Al15	146.3763	499.9465	Ga15	561.9992	1068.9999
Ti16	960.0092	749.6172	Ga16	1747.5429	410.6617	Al16	67.0637	589.7539	Al16	9.7640	345.3731
Ga17	1125.4109	1142.8250	Ti17	985.5186	680.7430	Ga17	1659.0550	416.7764	Al17	198.3902	451.1506
Al18	122.4984	486.4085	Ga18	1238.0104	1074.7605	Ti18	960.3130	718.7992	Ga18	2273.2970	1026.5069
Al19	5.8116	645.5896	Al19	248.2057	756.2451	Ga19	155.6199	1148.5059	Al19	163.6230	384.4612
Ga20	2814.7285	109.7524	Al20	237.4912	313.2766	Al20	149.7685	494.6129	H20	18.9590	61.9691

Table 1. (*Continued*).

BTA @Ti–(Al–Ga)			2MBT @Ti–(Al–Ga)			8HQ @Ti–(Al–Ga)			ATR @Ti–(Al–Ga)		
Atom	**σ_{iso}**	**σ_{aniso}**	**Atom**	**σ_{iso}**	**σ_{aniso}**	**Atom**	**σ_{iso}**	**σ_{aniso}**	**Atom**	**σ_{iso}**	**σ_{aniso}**
Al21	474.9763	288.6708	Ga21	2436.9743	563.7037	Al21	15.2227	711.2818	H21	28.9438	15.1633
H22	11.1800	47.3958	Al22	495.9512	512.5519	Ga22	2760.9758	207.2477	H22	29.1543	15.8472
H23	25.2346	4.9269	H23	26.1444	7.1234	Al23	451.3756	158.1253			
H24	24.5753	3.6723	H24	25.7183	5.9815	H24	25.0509	4.0106			
H25	25.3436	3.5121	H25	25.0572	6.2016	H25	25.8934	4.2494			
			H26	25.3752	5.5229	H26	25.1887	3.1011			
						H27	23.4236	7.8379			
						H28	25.7152	3.8937			
						H29	25.2200	4.4910			

In **Table 1**, "NMR" data has reported the notable amounts for transition metal of titanium which has been doped on the Al–Ga surface through the adsorption of BTA, 2MBT, 8HQ, and ATR heterocyclic carbenes.

In fact, the adsorption of BTA, 2MBT, 8HQ, and ATR heterocycles introduces spin polarization on the Ti–doped "Al–Ga" nanoalloy surface which indicates that this surface might be applied as magnetic sulfur and nitrogen heterocycle detectors. In fact, it is revealed that the "isotropic" and "anisotropy" shielding augment with the occupancy in BTA, 2MBT, 8HQ, and ATR heterocycles penetrated by "S- and N-atoms" in the benzene ring diffusing onto Ti–doped Al–Ga surface (**Figure 3a–d**).

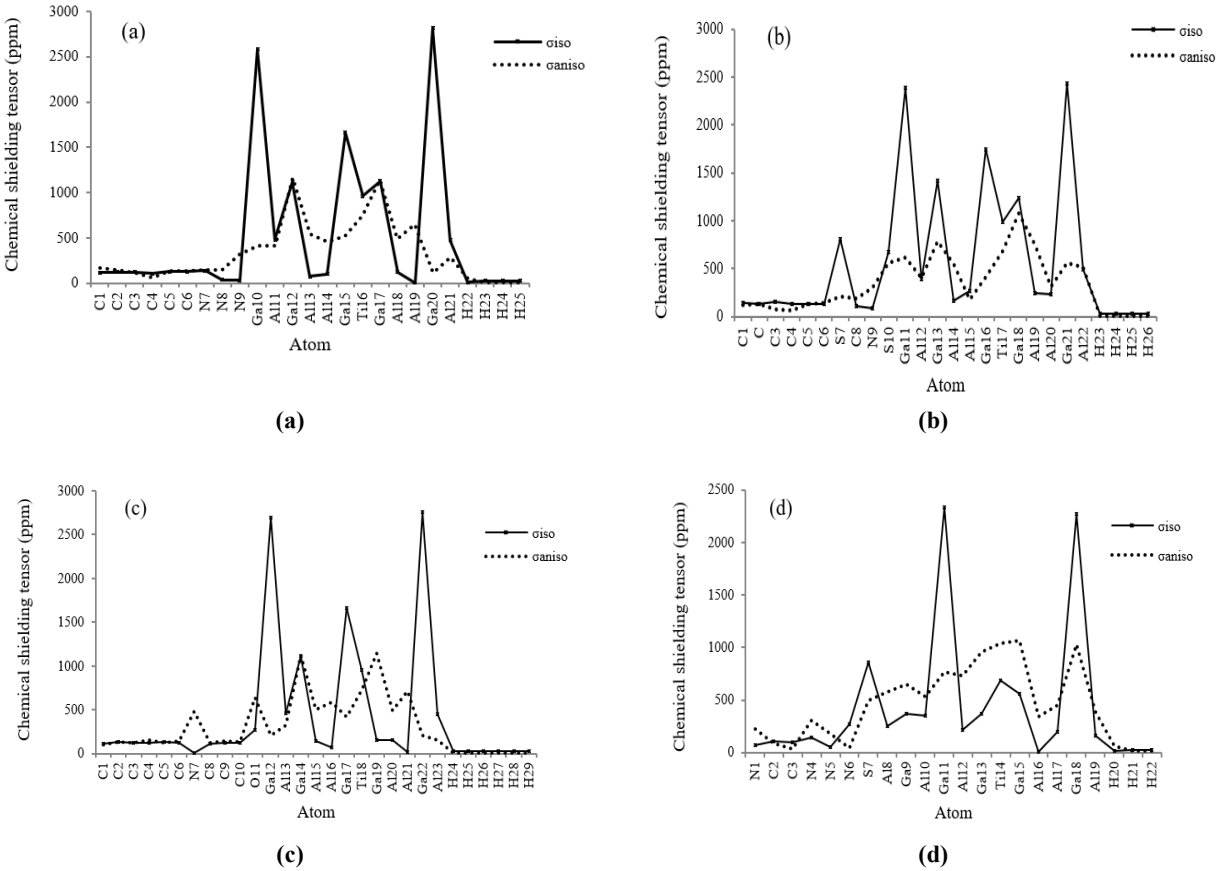

Figure 3. The NMR spectroscopy results of isotropic shielding tensor (σ_{iso}) and anisotropic shielding tensor (σ_{aniso}) of different elements in S–& N– heterocycles adsorbed on the Ti–doped Al–Ga: **(a)** BTA @Ti–(Al–Ga), **(b)** 2MBT @Ti–(Al–Ga), **(c)** 8HQ @Ti–(Al–Ga), and **(d)** ATR @Ti–(Al–Ga) complexes accompanying "CAM-B3LYP/EPR-III, LANL2DZ,6-31 + G(d,p)".

In **Figure 3a–d**, titanium in the complexes of BTA @Ti–(Al–Ga) (**Figure 3a**), 2MBT @Ti–(Al–Ga) (**Figure 3b**), 8HQ @Ti–(Al–Ga) (**Figure 3c**), and ATR @Ti–(Al–Ga) (**Figure 3d**) denotes the fluctuation in the chemical shielding tensor.

In fact, **Figure 3a–d** indicates the maximum fluctuation for gallium atoms in the neighboring of titanium in the center of metal alloy (adsorbent) for receiving the electrons of nitrogen (N→Ti), oxygen (O→Ti) and sulfur (S→Ti) of BTA, 2MBT, 8HQ, and ATR heterocycles (adsorbate).

3.3. Electrostatic properties & "NQR"

In this research, the calculated "nuclear quadrupole resonance" or "NQR" specifications extract from electrostatic properties have been calculated for BTA, 2MBT, 8HQ, and ATR which is accord to the results of the "nuclear quadrupole moment", a trait of the nucleus, and the "electric field gradient" or "EFG" in the neighborhood of the nucleus.

As the "EFG" at the citation of the nucleus in N-heterocycles is allocated by the valence electrons twisted in the particular attachment with close nuclei of Ti–doped "Al–Ga" alloy crystal, the "NQR" frequency at which transitions occur is particular for an (N-heterocycles) @(Ti–Al–Ga) complexes (**Table 2**). In "NMR", nuclei with *spin ≥1/2* have a magnetic dipole moment so that their energies are split by a magnetic field, permitting resonance sorption of energy dependent on the "Larmor frequency"; $\omega_L = \gamma B$, where γ is the gyromagnetic ratio and B is the magnetic field external to the nucleus. In "NQR", nuclei with spin ≥1, there is an electric quadrupole moment which is accompanied with "non-spherical" nuclear charge diffusions. So, the nuclear charge diffusion extracts from that of a sphere as the oblate or prolate form of the nucleus[77,78]. "NQR" is a straight frame of the interaction of the "quadrupole moment" with the "EFG" which is produced by the electronic structure of its ambiance. Therefore, the "NQR" transition frequencies are symmetric to the electric quadrupole moment of the nucleus and a measurement of the strength of the local "EFG": $\omega \sim \frac{e^2 Qq}{\hbar} = C_q$, where q is dependent on the biggest fundamental portion of the "EFG" tensor at the nucleus, and C_q is quadrupole coupling constant parameter[79,80].

In this research work, the "electric potential" as the quantity of work energy through carrying over the electric charge from one position to another position in the essence of electric field has been evaluated for BTA @Ti–(Al–Ga), 2MBT @Ti–(Al–Ga), 8HQ @Ti–(Al–Ga), and ATR @Ti–(Al–Ga) complexes using "CAM-B3LYP/EPR-III,LANL2DZ, 6-31+G(d,p)" level of theory (**Table 2**).

Table 2. The Bader charge (Q/e) and electric potential (Ep/a.u.) for elements of BTA, 2MBT,8HQ, and ATR which have been adsorbed on the Ti–(Al–Ga) alloy surface by CAM–B3LYP/EPR–III,6-31+G(d,p) calculation extracted of "NQR" method.

BTA @Ti–(Al–Ga)			**2MBT @Ti–(Al–Ga)**			**8HQ @Ti–(Al–Ga)**			**ATR @Ti–(Al–Ga)**		
Atom	**Q**	**E_p**	**Atom**	**Q**	**E_p**	**Atom**	**Q**	**E_p**	**Atom**	**Q**	**E_p**
C1	–0.1125	–14.6212	C1	–0.0664	–14.5063	C1	0.1210	–14.4825	N1	–0.2938	–18.1582
C2	–0.0808	–14.5659	C	–0.0754	–14.5231	C2	–0.1149	–14.5679	C2	0.2343	–14.4573
C3	0.0396	–14.5285	C3	–0.2057	–14.4938	C3	0.0336	–14.5392	C3	0.0121	–14.5179
C4	0.0402	–14.5359	C4	0.0861	–14.4747	C4	–0.0097	–14.5484	N4	–0.2280	–18.0638
C5	–0.0799	–14.5536	C5	–0.0665	–14.5232	C5	–0.1030	–14.5797	N5	–0.2079	–18.1454
C6	–0.0895	–14.5665	C6	–0.0726	–14.5245	C6	–0.0765	–14.5574	N6	–0.4049	–18.0294
N7	–0.1672	–18.0411	S7	0.3250	–58.1111	N7	–0.2343	–18.1153	S7	0.4273	–58.3342
N8	–0.0654	–18.0688	C8	–0.1770	–14.5121	C8	0.0077	–14.5279	Al8	0.2681	–43.5789
N9	–0.1613	–18.0865	N9	–0.2524	–18.0712	C9	–0.0882	–14.5578	Ga9	1.1136	–146.0595
Ga10	0.1207	–146.475	S10	0.3488	–58.3634	C10	–0.0767	–14.5525	Al10	–0.3685	–43.4074

Table 2. (*Continued*).

BTA @Ti–(Al–Ga)			2MBT @Ti–(Al–Ga)			8HQ @Ti–(Al–Ga)			ATR @Ti–(Al–Ga)		
Atom	**Q**	**E_p**	**Atom**	**Q**	**E_p**	**Atom**	**Q**	**E_p**	**Atom**	**Q**	**E_p**
Al11	–0.1053	–43.569	Ga11	0.0448	–146.495	O11	–0.2265	–21.9892	Ga11	0.4462	–146.4056
Ga12	0.9176	–146.166	Al12	–0.0527	–43.6163	Ga12	0.0589	–146.489	Al12	0.2801	–43.5816
Al13	0.3653	–43.669	Ga13	0.9627	–146.186	Al13	–0.0903	–43.6019	Ga13	0.9883	–146.0851
Al14	–0.0023	–43.6023	Al14	0.2255	–43.7377	Ga14	0.9542	–146.185	Ti14	–3.6262	–89.9952
Ga15	1.0241	–146.174	Al15	–0.0180	–43.6155	Al15	0.3439	–43.6835	Ga15	1.2081	–146.0879
Ti16	–3.2144	–90.1082	Ga16	0.9769	–146.177	Al16	–0.0163	–43.6093	Al16	–0.3449	–43.4154
Ga17	0.9187	–146.185	Ti17	–3.4484	–90.1336	Ga17	0.9868	–146.177	Al17	–0.4371	–43.3663
Al18	0.3749	−43.6645	Ga18	0.7519	–146.2	Ti18	–3.1653	–90.1096	Ga18	0.9428	–146.3735
Al19	–0.0369	–43.5944	Al19	0.3708	–43.6268	Ga19	0.9342	–146.203	Al19	–0.3634	–43.4365
Ga20	0.1057	–146.475	Al20	–0.0096	–43.6087	Al20	0.3506	–43.677	H20	–0.1165	–0.7069
Al21	–0.1060	–43.5684	Ga21	0.0430	–146.487	Al21	–0.0269	–43.6087	H21	0.2355	–1.0121
H22	0.0684	–1.06291	Al22	–0.0461	–43.605	Ga22	0.0742	–146.49	H22	0.2347	–1.0115
H23	0.0776	–1.1452	H23	0.0780	–1.08985	Al23	–0.1136	–43.5827			
H24	0.0925	–1.12976	H24	0.0867	–1.11231	H24	0.0725	–1.13396			
H25	0.0761	–1.14576	H25	0.1019	–1.10939	H25	0.0700	–1.15191			
			H26	0.0886	–1.11547	H26	0.0789	–1.13683			
						H27	0.0926	–1.13105			
						H28	0.0799	–1.13565			
						H29	0.0831	-1.12984			

Furthermore, in **Figure 4a–d**, it has been sketched the "Bader charge" for some atoms of hydrogen, carbon, nitrogen, oxygen, aluminum, gallium and titanium in the adsorption process of BTA, 2MBT, 8HQ, and ATR on the Ti-doped "Al–Ga" alloy surface which have been calculated by "CAM-B3LYP/EPR-III, 6-311 + G (d,p), LANL2DZ".

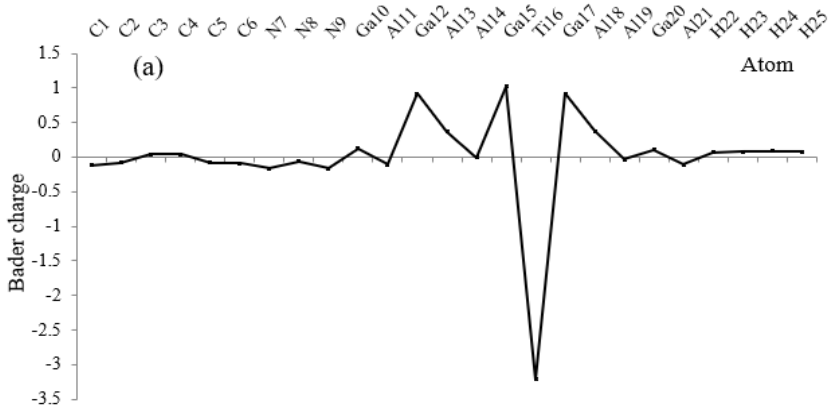

Figure 4. (*Continued*).

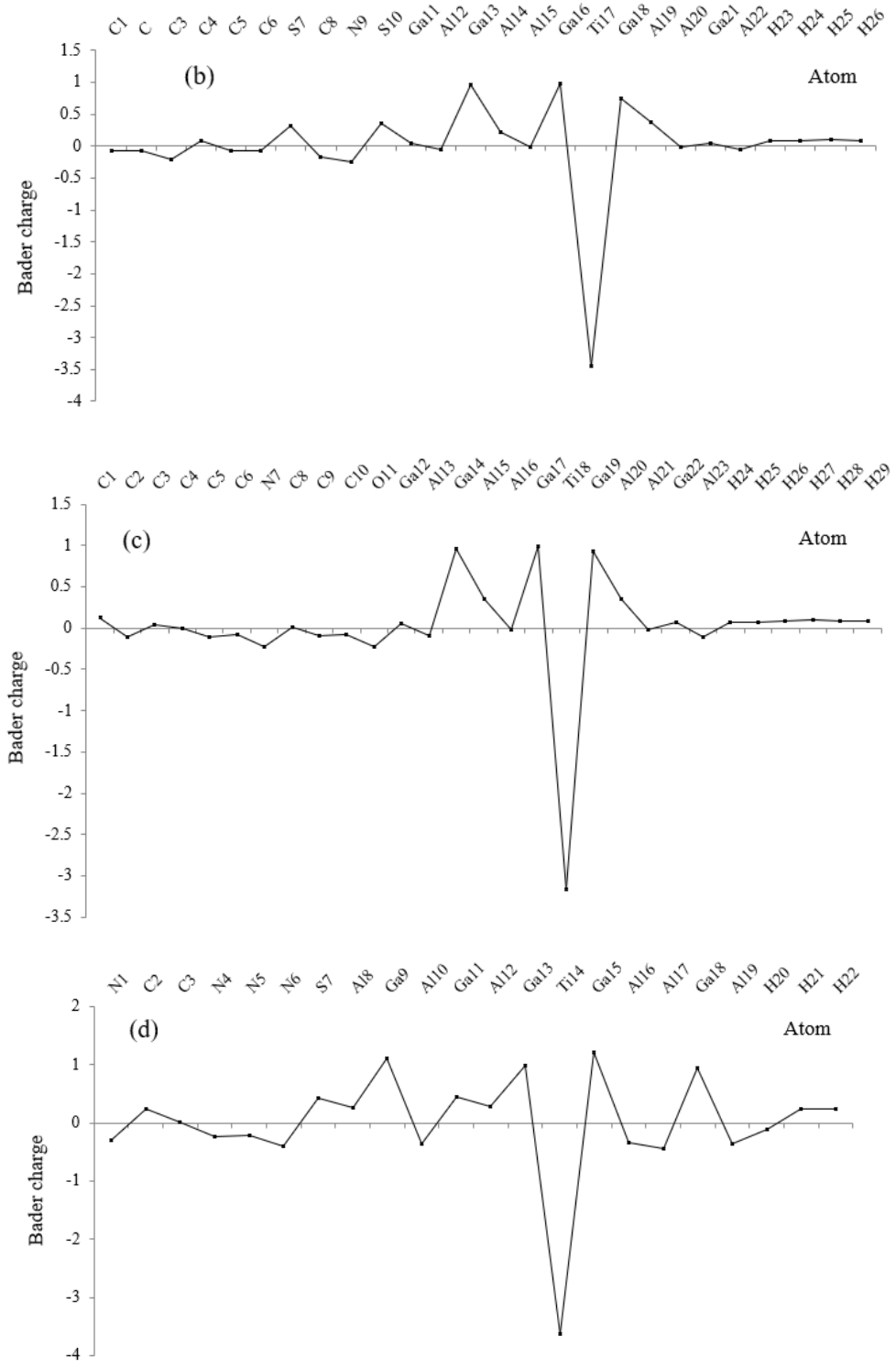

Figure 4. Bader charge (a.u.) atoms of H, C, N, O, Al, Ga and Ti in the adsorption process of **(a)** BTA, **(b)** 2MBT, **(c)** 8HQ, and **(d)**ATR on the Ti–doped "Al–Ga" alloy by "CAM-B3LYP/EPR-III, LANL2DZ,6-31 + G(d,p).

In **Figure 4a–d**, it has been described the influence of the replacement of aluminum metal elements in "Al–Ga" surface with "Ti". It's vivid that the curve of "Al–Ga" is waved by the transition metal. The sharpest peaks for Bader charge have been shown around transition metal doping of the Al–Ga which present the electron accepting characteristics of titanium versus nitrogen and sulfur atoms of heterocycles in BTA, 2MBT, 8HQ, and ATR (**Figure 4a–d**).

It has been exhibited that the Bader atomic charge graph of "S– and N–atoms" has the same tendency, however a considerable deviation from transition metal element of "Ti" (**Figure 4a–d**).

In fact, **Figure 4a–d** indicates that the gap Bader charge between N, S, O atoms and transitions metal "Ti" has the maximum value. On the other hand, it can be considered that the efficiency of electron accepting for the Ti–doped on the "Al–Ga" surface indicates the power of covalent bond between nitrogen, oxygen, sulfur and titanium.

The amounts of changes of charge density have exhibited a more important charge transfer from S- & N-heterocyclic inhibitors of BTA, 2MBT, 8HQ, and ATR as the electron donors adsorbed onto Ti–(Al–Ga) nanoalloy which play a role as the electron acceptor "S→Ti, N→Ti". In fact, "Ti" sites in "Ti–(Al–Ga)" nanoalloy has more interaction energy from "Van der Waals' forces" with BTA, 2MBT, 8HQ, and ATR that can cause more stability towards coating specifications on the alloy crystal. It has been estimated that the precedence for picking out the crystal binding of "N-, O-, S-atoms" in BTA, 2MBT, 8HQ, and ATR in adsorption positions can be impressed by the essence of neighboring elements of aluminum and gallium in the "Ti–(Al–Ga)" surface.

3.4. Infrared "IR" spectroscopy & thermodynamic analysis

The "IR" spectrums for adsorption of BTA, 2MBT, 8HQ, and ATR on the surfaces of Ti–doped on the "Al–Ga" have been reported in **Figure 5a–d**. The graphs of **Figure 5a–d** has been observed in the frequency range between 500 cm^{-1}–4500 cm^{-1} for the complexes of BTA @Ti–(Al–Ga), 2MBT @Ti–(Al–Ga), 8HQ @Ti–(Al–Ga), and ATR @Ti–(Al–Ga).

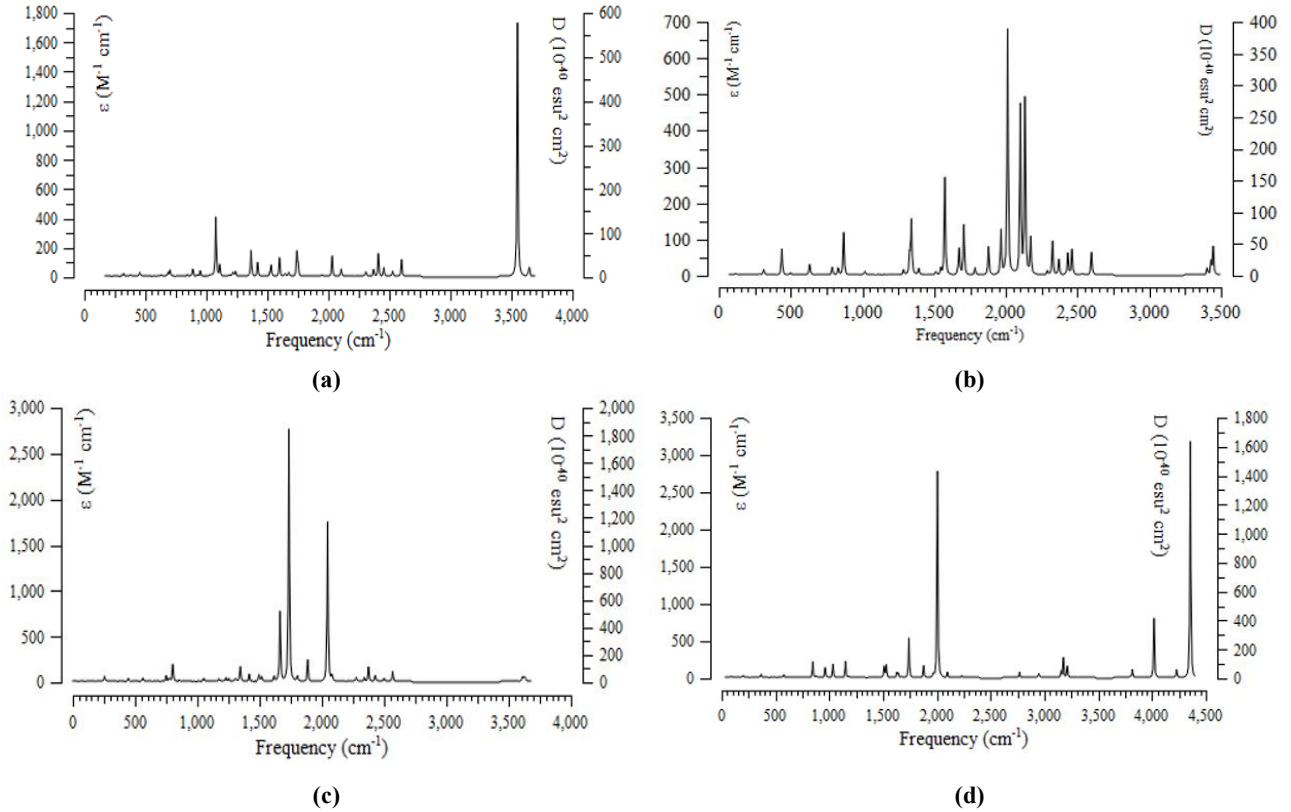

Figure 5. Infrared spectrums for titanium doping of aluminum–gallium nanosheet alloy as: **(a)** BTA @Ti–(Al–Ga), **(b)** 2MBT @Ti–(Al–Ga), **(c)** 8HQ @Ti–(Al–Ga), and **(d)** ATR @Ti–(Al–Ga).

The "IR" spectrum for each of these materials in **Figure 5a–d** has been observed in the maximum "frequency" approximately around 1000–3500 cm^{-1} with a sharp peak at 3500 cm^{-1} for BTA @Ti–(Al–Ga)

(**Figure 5a**), around 500–2500 cm^{-1} with three sharps peak at 2000 cm^{-1}, 2100 cm^{-1}, and 2150 cm^{-1} for 2MBT @Ti–(Al–Ga) (**Figure 5b**), around 1500–2250 cm^{-1} with two sharp peaks at 1725 cm^{-1} and 2050 cm^{-1} for 8HQ @Ti–(Al–Ga) (**Figure 5c**), around 1500–4500 cm^{-1} with two sharp peaks at 2000 cm^{-1} and 4350 cm^{-1} for ATR @Ti–(Al–Ga) (**Figure 5d**).

Furthermore, these materials have been accounted at "CAM-B3LYP" level of theory accompanying "6-31+G (d,p)/EPRIII/LANL2DZ" basis sets to receive the more valid equilibrium geometrical specifications, physical and thermodynamic parameter for each of the dedicated composition (**Table 3**).

Table 3. The physicochemical behavior of BTA, 2MBT, 8HQ, and ATR adsorbed on the Ti–(Al–Ga) surface and formation of BTA @Ti–(Al–Ga), 2MBT @Ti–(Al–Ga), 8HQ @Ti–(Al–Ga), and ATR @Ti–(Al–Ga) complexes.

Compound	$\Delta E^o \times 10^{-4}$ (kcal/mol)	$\Delta H^o \times 10^{-4}$ (kcal/mol)	$\Delta G^o \times 10^{-4}$ (kcal/mol)	S^o (cal/K.mol)	Dipole moment (Debye)
Ti–Al–Ga	–739.1685	–739.1685	–739.1708	79.167	7.0260
BTA	–24.5172	–24.5172	–24.5196	80.255	3.3166
2MBT	–69.5235	–69.5234	–69.5260	85.643	2.5108
8HQ	–29.5527	–29.5526	–29.5551	83.336	1.6389
ATR	-43.1336	–43.1336	–43.1358	73.839	1.5672
BTA @Ti–(Al–Ga)	–763.6316	–763.6316	–763.6343	90.194	7.1112
2MBT @Ti–(Al–Ga)	–808.5925	–808.5924	–808.5952	93.169	9.1414
8HQ @Ti–(Al–Ga)	–768.6825	–768.6824	–768.6855	101.515	6.6887
ATR@Ti–(Al–Ga)	–781.5880	–781.5879	–781.5906	90.766	6.5028

Based on **Table 3**, the thermodynamic specifications, the authors concluded that this protective film containing the (BTA, 2MBT, 8HQ, and ATR)@ Ti–(Al–Ga) which might be effective through doping of transition metal (Ti) toward formation of complexes including BTA @Ti–(Al–Ga), 2MBT @Ti–(Al–Ga), 8HQ @Ti–(Al–Ga), and ATR @Ti–(Al–Ga).

Considering **Figure 6**, it could be detected that the maximum of the "Langmuir adsorption isotherm" curves on the basis of ΔG^o_{ads} may depend on the interactions between the BTA, 2MBT, 8HQ, and ATR heterocycles and the "Ti–(Al–Ga)" alloy. Comparing the ΔG^o_{ads} amounts versus dipole moment can affirm a good accord among computed consequences and the validity of the picked isotherm for the adsorption procedure of BTA @Ti–(Al–Ga), 2MBT @Ti–(Al–Ga), 8HQ @Ti–(Al–Ga), and ATR @Ti–(Al–Ga) complexes (**Figure 6**).

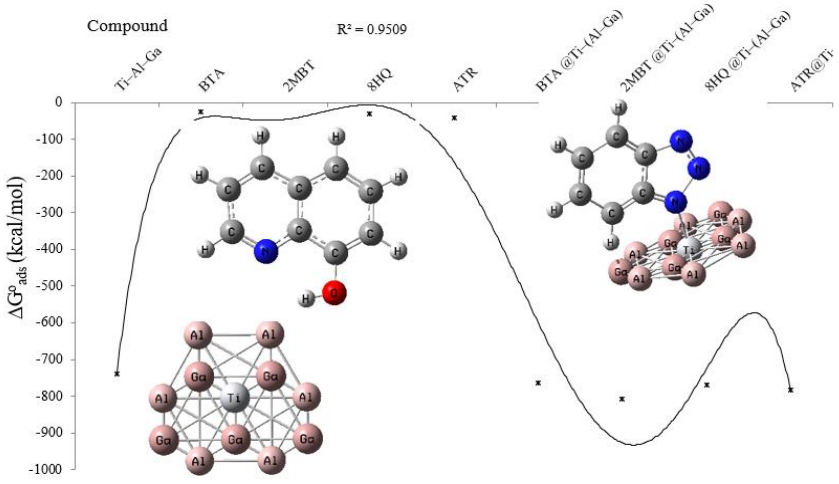

Figure 6. Gibbs free energy for adsorbing process of BTA, 2MBT, 8HQ, and ATR on "Ti–(Al–Ga)" alloy surface.

The "adsorptive capacity" of BTA, 2MBT, 8HQ, and ATR on the "Ti–(Al–Ga)" surface is affirmed by the ΔG^{o}_{ads} quantities:

$$\Delta G^{o}_{ads} = \Delta G^{o}_{adsorate@Ti-(Al-Ga)} - \left(\Delta G^{o}_{adsorbate} + \Delta G^{o}_{Ti-(Al-Ga)}\right) \quad (5)$$

Remarking **Table 3**, it is discovered that the adsorbing process of the S- & N-heterocyclic carbenes on the "Ti–(Al–Ga)" alloy might be physical and chemical nature. As seen in **Table 3**, all the accounted ΔG^{o}_{ads} amounts are very close, which demonstrate the agreement of the measured specifications by all methodologies and the reliability of the computing values.

Therefore, the interval between nitrogen, oxygen, sulfur atoms in BTA, 2MBT, 8HQ, and ATR during interaction and transition metal of "Ti" in "Ti–(Al–Ga)" nanoalloy, (N→Ti, O→Ti, S→Ti), has been estimated with relation coefficient of $R^2 = 0.9509$ (**Table 3** and **Figure 6**).

4. Conclusion

This study has analyzed the molecular properties of Al–Ga and the difference in its properties when doped with Transition metal "Ti". In this work, the adsorbing process and penetration of BTA, 2MBT, 8HQ, and ATR on the Ti-doped Al–Ga crystals have been studied based on "Langmuir theory" using "ONIOM" methodology with "*high*, *medium* and *low"* levels of "EPR-III/6-31 + G(d,p)/LANL2DZ", "semi-empirical" and "MM2" force fields accompanying "Gaussian 16 revision C.01".

Denoting this research, the efficiency of the S- & N-heterocyclic carbenes" as the inhibiting agents for Ti–(Al–Ga) has been investigated through the electromagnetic and thermochemical traits extracts from "PDOS", "NMR", "NQR", "IR" analysis which have been performed on BTA @Ti–(Al–Ga), 2MBT @Ti–(Al–Ga), 8HQ @Ti–(Al–Ga), and ATR @Ti–(Al–Ga) complexes.

In the preferred path, these S- & N-heterocyclic carbenes of BTA, 2MBT, 8HQ, and ATR stay collateral to the plane so long as fulfilling small single rotational steps with a "C–C" double bond belonged above a single transition metal element in "Ti–(Al–Ga)" nanoalloy. The inhibiting process of the protonated BTA, 2MBT, 8HQ, and ATR compositions is quoted to the total of the pure charge and the "π charge "of the "six-ring". BTA, 2MBT, 8HQ, and ATR have been adsorbed on the crystal surface of the "Ti–(Al–Ga)" electrodes primarily in their protonated shapes. The most eventual adsorption pattern of the inhibiting materials is one in which the "S- &N-atoms" of the BTA, 2MBT, 8HQ, and ATR are close to the Ti–doped of Al–Ga nanoalloy surface in an inclined state.

Author contributions

Conceptualization and idea, FM; methodology, FM and MM; software, FM and MM; validation, FM; formal analysis, FM and MM; resources, MM; investigation, FM and MM; data curation, FM and MM; writing—original draft preparation, FM; writing—review and editing, MM; visualization, FM and MM; supervision FM; project administration, FM. All authors have read and agreed to the published version of the manuscript.

Acknowledgments

In successfully completing this paper and its research, the authors are grateful to Kastamonu University for their support through the office, library, and scientific websites.

Conflict of interest

The authors declare no conflict of interest.

References

1. Ahmad Z. Principles of Corrosion Engineering and Corrosion Control. Butterworth-Heinemann; 2006.
2. Wei C. Electrochemical deposition of aluminum (Chinese). Technological Innovation and Application 2019; 18: 80–81.
3. Yang HM, Qiu ZX, Zhang G. Low Temperature Aluminum Electrolysis (Chinese); Northeast University Press; 2009.
4. Lu HM, Qiu ZX. Research progress of low temperature aluminum electrolysis (Chinese). Light Metals 1997; 4: 27–29.
5. Machnikova E, Whitmire KH, Hackerman N. Corrosion inhibition of carbon steel in hydrochloric acid by furan derivatives. Electrochimica Acta 2008; 53(20): 6024–6032. doi: 10.1016/j.electacta.2008.03.021
6. Benabdellah M, Touzani R, Aouniti A, et al. Inhibitive action of some bipyrazolic compounds on the corrosion of steel in 1M HCl. Materials Chemistry and Physics 2007; 105(2–3): 373–379. doi: 10.1016/j.matchemphys.2007.05.001
7. Fiala A, Chibani A, Darchen A, et al. Investigations of the inhibition of copper corrosion in nitric acid solutions by ketene dithioacetal derivatives. Applied Surface Science 2007; 253(24): 9347–9356. doi: 10.1016/j.apsusc.2007.05.066
8. Prabhu RA, Shanbhag AV, Venkatesha TV. Influence of tramadol [2-[(dimethylamino)methyl]-1-(3-methoxyphenyl) cyclohexanol hydrate] on corrosion inhibition of mild steel in acidic media. Journal of Applied Electrochemistry 2007; 37(4): 491–497. doi: 10.1007/s10800-006-9280-2
9. Tian G, Li J, Hua Y. Application of ionic liquids in metallurgy of nonferrous metals (Chinese). Chinese Journal of Process Engineering 2009; 1: 9. doi: 10.3321/j.issn:1009-606X.2009.01.039
10. Tian G, Li J, Hua Y. Application of ionic liquids in hydrometallurgy of nonferrous metals. Transactions of Nonferrous Metals Society of China 2010; 20(3): 513–520. doi: 10.1016/S1003-6326(09)60171-0
11. Monajjemi M, Afsharnezhad S, Jaafari MR, et al. Investigation of energy and NMR isotropic shift on the internal rotation Barrier of Θ4 dihedral angle of the DLPC: A GIAO study. Chemistry 2008; 16(3): 55–69.
12. Tian GC. Ionic liquids as green electrolytes for Aluminum and Aluminum-alloy production. Materials Research Foundations 2019; 54: 249–293. doi: 10.21741/9781644900314-11
13. Zhong X, Xiong T, Lu J, et al. Advances of electro-deposition and aluminum refining of aluminum and aluminum alloy in ionic liquid electrolytes system (Chinese). Nonferrous Metals Science and Engineering 2014; 5(2): 8. doi: 10.13264/j.cnki.ysjskx.2014.02.008
14. Zheng Y, Wang Q, Zheng Y, Lv H. Advances in research and application of aluminum electrolysis in ionic liquid systems (Chinese). Chinese Journal of Process Engineering 2015; 15(4): 8.
15. Fleury V, Kaufman JH, Hibbert DB. Mechanism of a morphology transition in ramified electrochemical growth. Nature 1994; 367(6462): 435–438. doi: 10.1038/367435a0
16. Yue G, Lu X, Zhu Y, et al. Surface morphology, crystal structure and orientation of aluminium coatings electrodeposited on mild steel in ionic liquid. Chemical Engineering Journal 2009; 147(1): 79–86. doi: 10.1016/j.cej.2008.11.044
17. Barth JV, Brune H, Ertl G, Behm RJ. Scanning tunneling microscopy observations on the reconstructed Au(111) surface: Atomic structure, long-range superstructure, rotational domains, and surface defects. Physical Review B 1990; 42(15): 9307–9318. doi: 10.1103/physrevb.42.9307
18. Esken D, Turner S, Lebedev OI, et al. Au@ZIFs: Stabilization and encapsulation of cavity-size matching gold clusters inside functionalized zeolite imidazolate frameworks, ZIFs. Chemistry of Materials 2010; 22(23): 6393–6401. doi: 10.1021/cm102529c
19. Mollaamin F, Monajjemi M. Fractal dimension on carbon nanotube-polymer composite materials using percolation theory. Journal of Computational and Theoretical Nanoscience 2012; 9(4): 597–601. doi: 10.1166/jctn.2012.2067
20. Liu B, Smit B. Molecular simulation studies of separation of CO_2/N_2, CO_2/CH_4, and CH_4/N_2 by ZIFs. The Journal of Physical Chemistry C 2010; 114(18): 8515–8522. doi: 10.1021/jp101531m
21. Keskin S. Atomistic simulations for adsorption, diffusion, and separation of gas mixtures in zeolite imidazolate frameworks. Journal of Physical Chemistry C 2010; 115(3): 800–807. doi: 10.1021/jp109743e
22. Tran UPN, Le KKA, Phan NTS. Expanding applications of metal-organic frameworks: Zeolite imidazolate framework ZIF-8 as an efficient heterogeneous catalyst for the Knoevenagel reaction. ACS Catalysis 2011; 1(2): 120–127. doi: 10.1021/cs1000625
23. VandeVondele J, Krack M, Mohamed F, et al. Quickstep: Fast and accurate density functional calculations using a mixed Gaussian and plane waves approach. Computer Physics Communications 2005; 167(2): 103–128. doi: 10.1016/j.cpc.2004.12.014
24. Phan A, Doonan CJ, Uribe-Romo FJ, et al. Synthesis, structure, and carbon dioxide capture properties of zeolitic imidazolate frameworks. Accounts of Chemical Research 2009; 43(1): 58–67. doi: 10.1021/ar900116g
25. Hohenberg P, Kohn W. Inhomogeneous electron gas. Physical Review Journals 1964; 136(3B): B864–B871. doi: 10.1103/physrev.136.b864

26. Kohn W, Sham LJ. Self-consistent equations including exchange and correlation effects. Physical Review Journals 1965; 140(4A): A1133–A1138. doi: 10.1103/physrev.140.a1133
27. Lippert G, Hutter J, Parrinello M. A hybrid Gaussian and plane wave density functional scheme. Molecular Physics 1997; 92(3): 477–487. doi: 10.1080/00268979709482119
28. Hartwigsen C, Goedecker S, Hutter J. Relativistic separable dual-space Gaussian pseudopotentials from H to Rn. Physical Review B 1998; 58(7): 3641–3662. doi: 10.1103/physrevb.58.3641
29. Perdew JP, Burke K, Ernzerhof M. Generalized gradient approximation made simple. Physical Review Letters 1996; 77(18): 3865–3868. doi: 10.1103/physrevlett.77.3865
30. VandeVondele J, Hutter J. Gaussian basis sets for accurate calculations on molecular systems in gas and condensed phases. The Journal of Chemical Physics 2007; 127(11): 114105-1–110105-9. doi: 10.1063/1.2770708
31. Monajjemi M, Mahdavian L, Mollaamin F. Characterization of nanocrystalline silicon germanium film and nanotube in adsorption gas by Monte Carlo and Langevin dynamic simulation. Bulletin of the Chemical Society of Ethiopia 2008; 22(2): 277–286. doi: 10.4314/bcse.v22i2.61299
32. Mavrikakis M, Stoltze P, Nørskov JK. Making gold less noble. Catalysis Letters 2000; 64: 101–106. doi: 10.1023/A:1019028229377
33. Dal Corso A. Ab initio phonon dispersions of transition and noble metals: Effects of the exchange and correlation functional. Journal of Physics: Condensed Matter 2013; 25(14): 145401. doi: 10.1088/0953-8984/25/14/145401
34. Subhadarshini S, Singh R, Mandal A, et al. Silver nanodot decorated dendritic copper foam as a hydrophobic and mechano-chemo bactericidal surface. Langmuir 2021; 37(31): 9356–9370. doi: 10.1021/acs.langmuir.1c00698.
35. Mollaamin F, Baei MT, Monajjemi M, et al. A DFT study of hydrogen chemisorption on V (100) surfaces. Russian Journal of Physical Chemistry A 2008; 82(13): 2354–2361. doi: 10.1134/s0036024408130323
36. Yildirim H, Greber T, Kara A. Trends in adsorption characteristics of benzene on transition metal surfaces: Role of surface chemistry and van der Waals interactions. Journal of Physical Chemistry C 2013; 117(40): 20572–20583. doi: 10.1021/jp404487z
37. Monajjemi M, Baie MT, Mollaamin F. Interaction between threonine and cadmium cation in $[Cd(Thr)\ n\ ]^{2+}$ (n = 1–3) complexes: Density functional calculations. Russian Chemical Bulletin 2010; 59(5): 886–889. doi: 10.1007/s11172-010-0181-5
38. Hoefling M, Iori F, Corni S, Gottschalk K. The conformations of amino acids on a Gold(111) surface. ChemPhysChem 2010; 11(8): 1763–1767. doi: 10.1002/cphc.200900990
39. Bakhshi K, Mollaamin F, Monajjemi M. Exchange and correlation effect of hydrogen chemisorption on nano V(100) surface: A DFT study by generalized gradient approximation (GGA). Journal of Computational and Theoretical Nanoscience 2011; 8(4): 763–768. doi: 10.1166/jctn.2011.1750
40. Valencia H, Kohyama M, Tanaka S, Matsumoto H. Ab initio study of EMIM-BF4 crystal interaction with a Li (100) surface as a model for ionic liquid/Li interfaces in Li-ion batteries. The Journal of Chemical Physics 2009; 131(24): 244705. doi: 10.1063/1.3273087
41. Clarke-Hannaford J, Breedon M, Best AS, Spencer MJS. The interaction of ethylammonium tetrafluoroborate $[EtNH_3^+][BF_4^-]$ ionic liquid on the Li(001) surface: Towards understanding early SEI formation on Li metal. Physical Chemistry Chemical Physics 2019; 21(19): 10028–10037. doi: 10.1039/c9cp01200a
42. Zhang Q. Study on Electrodeposition of Aluminum and Aluminum Alloy in Ionic Liquid (Chinese) [PhD thesis]. University of Chinese Academy of Sciences; 2014.
43. Mollaamin F, Monajjemi M. Harmonic linear combination and normal mode analysis of semiconductor nanotubes vibrations. Journal of Computational and Theoretical Nanoscience 2015; 12(6): 1030–1039. doi: 10.1166/jctn.2015.3846
44. Ali SA, Mazumder MAJ, Nazal MK, Al-Muallem HA. Assembly of succinic acid and isoxazolidine motifs in a single entity to mitigate CO_2 corrosion of mild steel in saline media. Arabian Journal of Chemistry 2020; 13(1): 242–257. doi: 10.1016/j.arabjc.2017.04.005
45. Amar H, Benzakour J, Derja A, et al. A corrosion inhibition study of iron by phosphonic acids in sodium chloride solution. Journal of Electroanalytical Chemistry 2003; 558: 131–139. doi: 10.1016/S0022-0728(03)00388-7
46. El-Sayed MS. Corrosion and corrosion inhibition of aluminum in Arabian Gulf seawater and sodium chloride solutions by 3-amino-5-mercapto-1,2,4-triazole. International Journal of Electrochemical Science 2011; 6(5): 1479–1492. doi: 10.1016/S1452-3981(23)15087-5
47. El-Sayed MS. A comparative study on the electrochemical corrosion behavior of iron and X-65 steel in 4.0 wt % sodium chloride solution after different exposure intervals. Molecules 2014; 19(7): 9962–9974. doi: 10.3390/ molecules19079962
48. Yang D, Zhang M, Zheng J, Castaneda H. Corrosion inhibition of mild steel by an imidazolium ionic liquid compound: the effect of pH and surface pre-corrosion. RSC Advances 2015; 5(115): 95160–95170. doi: 10.1039/C5RA14556B
49. Finšgar M, Milošev I. Inhibition of copper corrosion by 1,2,3-benzotriazole: A review. Corrosion Science 2010; 52(9): 2737–2749. doi: 10.1016/j.corsci.2010.05.002
50. Kothari DH, Kanchan DK. Study of study of electrical properties of gallium-doped lithium titanium aluminum phosphate compounds. Ionics 2014; 21(5): 1253–1259. doi: 10.1007/s11581-014-1287-9

51. Subhadarshini S, Pavitra E, Rama Raju GS, et al. One-pot facile synthesis and electrochemical evaluation of selenium enriched cobalt selenide nanotube for supercapacitor application. Ceramics International 2021; 47(11): 15293–15306. doi: 10.1016/j.ceramint.2021.02.093
52. Monajjemi M, Mollaamin F, Gholami MR, et al. Quantum chemical parameters of some organic corrosion inhibitors, pyridine, 2-picoline 4-picoline and 2,4-lutidine, adsorption at aluminum surface in hydrocholoric and nitric acids and comparison between two acidic media. Main Group Metal Chemistry 2003; 26(6): 349–362. doi: 10.1515/mgmc.2003.26.6.349
53. Mollaamin F, Shahriari S, Monajjemi M, Khalaj Z. Nanocluster of aluminum lattice via organic inhibitors coating: A study of freundlich adsorption. Journal of Cluster Science 2022; 34(3): 1547–1562. doi: 10.1007/s10876-022-02335-1
54. Mollaamin F, Monajjemi M. Corrosion inhibiting by some organic heterocyclic inhibitors through langmuir adsorption mechanism on the Al-X (X = Mg/Ga/Si) Alloy Surface: A study of quantum three-layer method of CAM-DFT/ONIOM. Journal of Bio- and Tribo-Corrosion 2023; 9(2): 33. doi: 10.1007/s40735-023-00751-y
55. Mollaamin F, Monajjemi M. Molecular modelling framework of metal-organic clusters for conserving surfaces: Langmuir sorption through the TD-DFT/ONIOM approach. Molecular Simulation 2022; 49(4): 365–376. doi: 10.1080/08927022.2022.2159996
56. Mollaamin F, Monajjemi M. In Silico-DFT investigation of nanocluster alloys of Al-(Mg, Ge, Sn) coated by nitrogen heterocyclic carbenes as corrosion inhibitors. Journal of Cluster Science 2023. doi: 10.1007/s10876-023-02436-5.
57. Zupanič F, Žist S, Albu M, et al. Dispersoids in Al-Mg-Si alloy AA 6086 modified by Sc and Y. Materials 2023; 16(8): 2949. doi: 10.3390/ma16082949
58. Li S, Dong H, Wang X, Liu Z. Quenching sensitivity of Al-Zn-Mg alloy after non-isothermal heat treatment. Materials 2019; 12(10): 1595. doi: 10.3390/ma12101595
59. Wang Z, Zhang P, Zhao X, Rao S. The corrosion behavior of Al-Cu-Li alloy in NaCl solution. Coatings 2022; 12(12): 1899. doi: 10.3390/coatings12121899
60. Amberchan G, Lopez I, Ehlke B, et al. Aluminum nanoparticles from a Ga–Al composite for water splitting and hydrogen generation. ACS Applied Nano Materials 2022; 5(2): 2636–2643. doi: 10.1021/acsanm.1c04331
61. Svensson M, Humbel S, Froese RDJ, et al. ONIOM: A multilayered integrated MO + MM method for geometry optimizations and single point energy predictions. A test for diels-alder reactions and $Pt(P(t\text{-}Bu)_3)_2 + H_2$ oxidative addition. The Journal of Physical Chemistry 1996; 100(50): 19357–19363. doi: 10.1021/jp962071j
62. Mingdao,L, Lu-An, Y, Qing, Y, et al. A study on correlation between electronic structure and inhibition properties of five-membered dinitrogen heterocyclic compounds. Journal of Chinese Society of Corrosion and Protection 1996; 16(3): 195-200.
63. Brandt F, Jacob CR. Systematic QM region construction in QM/MM calculations based on uncertainty quantification. Journal of Chemical Theory and Computation 2022; 18(4): 2584–2596. doi: 10.1021/acs.jctc.1c01093
64. Blöchl PE. Projector augmented-wave method. Physical Review B 1994; 50(24): 17953–17979. doi: 10.1103/physrevb.50.17953
65. Perdew JP, Burke K, Ernzerhof M. Generalized gradient approximation made simple. Physical Review Letters 1996; 77(18): 3865–3868. doi: 10.1103/physrevlett.77.3865
66. Ziesche P, Kurth S, Perdew JP. Density functionals from LDA to GGA. Computational Materials Science 1998; 11(2): 122–127. doi: 10.1016/S0927-0256(97)00206-1
67. Arrigoni M, Madsen GKH. Comparing the performance of LDA and GGA functionals in predicting the lattice thermal conductivity of III-V semiconductor materials in the zincblende structure: The cases of AlAs and BAs. Computational Materials Science 2019; 156: 354–360. doi: 10.1016/j.commatsci.2018.10.005
68. Becke AD. Density-functional thermochemistry. III. The role of exact exchange. The Journal of Chemical Physics 1993; 98(7): 5648–5652. doi: 10.1063/1.464913
69. Lee C, Yang W, Parr RG. Development of the Colle-Salvetti correlation-energy formula into a functional of the electron density. Physical Review B 1988; 37(2): 785–789. doi: 10.1103/physrevb.37.785
70. Kim K, Jordan KD. Comparison of density functional and MP2 calculations on the water monomer and Dimer. The Journal of Physical Chemistry 1994; 98(40): 10089–10094. doi: 10.1021/j100091a024
71. Stephens PJ, Devlin FJ, Chabalowski CF, Frisch MJ. Ab initio calculation of vibrational absorption and circular dichroism spectra using density functional force fields. The Journal of Physical Chemistry 1994; 98(45): 11623–11627. doi: 10.1021/j100096a001
72. Cramer CJ. Essentials of Computational Chemistry: Theories and Models, 2nd ed. Wiley; 2004.
73. Vosko SH, Wilk L, Nusair M. Accurate spin-dependent electron liquid correlation energies for local spin density calculations: a critical analysis. Canadian Journal of Physics 1980; 58(8): 1200–1211. doi: 10.1139/p80-159
74. Frisch MJ, Trucks GW, Schlegel HB, et al. Gaussian 16, Revision C.01, Gaussian, Inc., Wallingford CT, 2016. Available online: https://gaussian.com/ (accessed on 24 September 2021).
75. Dennington R, Keith TA, Millam J. GaussView Version 6. Available online: https://gaussian.com/gaussview6/ (accessed on 11 February 2023).

76. Sohail U, Ullah F, Binti Zainal Arfan NH, et al. Transition metal sensing with nitrogenated holey graphene: A first-principles investigation. Molecules 2023; 28(10): 4060. doi: 10.3390/molecules28104060
77. Smith JAS. Nuclear quadrupole resonance spectroscopy. Journal of Chemical Education 1971; 48: 39–41.
78. Garroway AN. Nuclear quadrupole resonance. Available online: https://studylib.net/doc/12810542/nuclear-quadrupole-resonance--paper-ii--introduction--nuc. (accessed on 25 October 2023).
79. Poleshchuck OK, Kalinna EL, Latosinska JN, Koput J. Application of density functional theory to the analysis of electronic structure and quadrupole interaction in dimers of transition and non-transition elements. Journal of Molecular Structure: THEOCHEM 2001; 547(1–3): 233–243. doi: 10.1016/S0166-1280(01)00636-4
80. Young HA, Freedman RA. Sears and Zemansky's University Physics with Modern Physics, 13th ed. Addison-Wesley; 2012. p. 754.